INDC (IND) 007G

INDC #274

B.A.R.C.-363

B.A.R.C.-363

सत्यमेव जयते

GOVERNMENT OF INDIA
ATOMIC ENERGY COMMISSION

YIELD OF K X-RAYS EMITTED FROM U^{236} FRAGMENTS

by

S. S. Kapoor, V. S. Ramamurthy and R. Zaghloul
(Nuclear Physics Division)

BHABHA ATOMIC RESEARCH CENTRE
BOMBAY, INDIA
1968

B.A.R.C.-363

B.A.R.C.-363

GOVERNMENT OF INDIA
ATOMIC ENERGY COMMISSION

YIELD OF K X-RAYS EMITTED FROM U^{236} FRAGMENTS

by
S.S. Kapoor, V.S.Ramamurthy and R. Zaghloul
(Nuclear Physics Division)

BHABHA ATOMIC RESEARCH CENTRE
BOMBAY, INDIA
1968

ABSTRACT

The yield of K x-rays from different fragment masses have been determined in the thermal neutron induced fission of U^{235}. The energies of the pairs of fragments were measured with two semi-conductor detectors placed on either side of a thin U^{235} foil. The K x-rays from the light and the heavy groups of fragments were separated by measuring the x-ray energies with a 1 mm NaI(Tl) crystal. The fragment mass distributions in coincidence with the light group of K x-rays, heavy group of K x-rays and the unbiased mass distributions were simultaneously recorded in different quarters of a 1024 channel analyser memory. From these distributions, after suitable corrections for the background, x-ray detection efficiencies and finite energy resolution effects, the number of x-rays as a function of fragment mass have been determined. The K x-ray yield per fission is found to be (0.08 ± 0.01) for the light fragment group, and (0.30 ± 0.02) for the heavy fragment group. The gross features of the yield as a function of mass are similar to those observed earlier for emission from Cf^{252} fragments. However, unlike the case of Cf^{252}, for masses greater than 144 the striking increase in the yield is not observed. The present results are consistent with the interpretation that the x-ray yield depends both on the characteristics of the low lying states and the initial spin of the fragments.

fission chamber through two aluminised Mylar windows to avoid scattering of the beam at the chamber walls. The U^{235} foil was mounted on a rod fixed at an angle of 45° to the top plate of the chamber in such a way that the foil was at an angle of 45° each to the incident beam, the line joining the fission detectors and the line joining the center of the foil and the x-ray detector. The x-rays were detected through a 0.01 in. beryllium window of 1.25 in. diameter fixed at the centre of the base plate of the chamber. In this geometry the distance of the NaI(Tl) crystal from the center of the foil was fixed at 8.1 cm.

B. Procedure and Electronics

The method consisted in simultaneously measuring the fragment mass distributions in coincidence with the light group of K x-rays, heavy group of K x-rays and without regard to any secondary radiations. From these distributions, after correction for the background, x-ray detection efficiencies and the finite energy resolution effects, the K x-ray yield as a function of fragment mass were obtained. Fig.2 shows the block diagram of the electronic arrangement. The pulse height distributions from the fission detectors, D_1 and D_2 were first matched by adjusting the amplifier gains. The amplified pulse heights V_1 and V_2 from detectors D_1 and D_2 respectively were then fed to an adder divider circuit which generated a pulse proportional to $V_2/(V_1+V_2)$. As also pointed out by Atneoson et al[3], because of the observed linear dependence of the pulse height defect with fragment mass, $V_2/(V_1+V_2)$ is linearly related to $E_2/(E_1 + E_2)$ where E_1 and E_2 are the kinetic energies of the pair fragments. From the conservation of momentum it follows that the output $V_2/(V_1+V_2)$ is proportional to the fragment mass M_1, if it is assumed that no neutrons were emitted from the fragments. The procedure adopted for the calibration of $V_2/(V_1+V_2)$ versus fragment mass and the correction of the mass distribution for the effects of neutron emission and experimental mass dispersion are described in the Appendix. The output of adder-divider circuit was fed to a 1024 channel analyser, divided into four quarters of 256 channels each. The mass distribution without coincidence with any secondary radiation was recorded in the first quarter of the analyser memory.

The pulse heights from the x-ray detector were calibrated into energies using the sources of Am^{241}, Co^{57}, Cs^{137}, Ba^{133} and Gd^{153}. The full width at half maximum (FWHM) of the Ba K_{α} line was found to be about 10.0 kev. The relationship between energy resolution of the x-ray detector system and the photon energy was also experimentally obtained using the calibration sources. A high precision pulser fed at the input of the x-ray detector amplifier was also calibrated with respect to x-ray energies. The pulse heights from the x-ray detector system corresponding to the light fragment K x-ray energy group (8 to 21.1 kev) and the heavy fragment K x-ray energy group (21.1 to 50 kev) were selected with two single channel analysers using the calibrated pulser. The pulses from the fission detector D_2 and the x-ray detector were fed to a coincidence unit of resolution time (2τ) of 1.2 μsec to ensure 100% coincidence efficiency. The single channel analyser outputs were gated with the coincidence pulse to select the light and heavy fragment K x-rays respectively. These pulses selecting light and heavy fragment K x-rays were used to steer the pulse height analyser so that if there was a pulse corresponding to the detected light fragment or heavy fragment K x-ray, the $V_2/(V_1 + V_2)$ output was stored in the 2/4 or 3/4 of the analyser memory respectively instead of in the 1/4 quarter. In this way, the data recorded simultaneously in the 1/4, 2/4 and 3/4 of the analyser memory represented the normal fragment mass distribution, mass distribution in coincidence with light fragment K x-rays and in coincidence with heavy fragment K x-rays respectively. The K x-ray spectrum was also recorded periodically by gating the NaI(Tl) detector output with the fragment x-ray coincidence pulse.

In 15 separate runs of 24 hours each, about 10^5 triple coincidence events corresponding to 2.36×10^7 binary events were recorded. To ensure the stability of the selected energy windows, the energy calibration of the precision pulser and the settings of the two single channel analysers were checked before and after each run.

C. Background Corrections

The above measurements were carried out with and without a copper filter of thickness 440 mg/cm^2 to correct for the background triple coincidences. This filter was essentially opaque to the fragment K x-rays (10 - 40 kev) and was practically transparent for the fission γ-rays. The transmission of this absorber for 30 kev, 40 kev and 100 kev photons was calculated to the (0.8)%, (12.3)% and (82.0)% respectively. The measurements taken with the absorber represented total background counts arising firstly due to the true coincidences between fission and the compton scattered fission γ-rays, and secondly due to the chance coincidences. The difference between these two measurements represented to a good approximation the spectra in coincidence with the K x-rays alone. A small transmission of the high energy K x-rays ($\sim$ 40 kev) through this filter was taken into account in correcting for the background. Measurements showed that about 40% of the total counts belonged to the background coincidences, the chance coincidences being only 15% of the total.

III. RESULTS AND ANALYSIS

The observed energy distributions of the x-rays after correction for the background is shown in Fig.3. This measurement was done earlier[10] in an experimental geometry different from that shown in Fig.1. In this case the x-ray detector was in line with the fragment detector placed on the other side of the foil. This spectrum contains the x-rays emitted from both members of the fragment pair, one moving towards and the other away from the x-ray detector and hence the Doppler shifts on the average energies is not expected. The spectrum of the x-rays emitted from Cf^{252} fragments as measured by Glendenin and Griffin[(1)] with a NaI(Tl) detector is also shown in the figure for the sake of comparison of peak positions in the two cases.

The mass distributions $Y_x^L(M)$ and $Y_x^L(M)$ observed in coincidence with the light group and heavy group of K x-rays are shown in Fig.4 along with the normal mass distribution $Y(M)$. Here M is the approximate preneutron emission mass, uncorrected for the effects of neutron emission and mass dispersion. The second hump in the distribution $Y_x^L(M)$ and the first hump in the distribution $Y_x^H(M)$ correspond to the cases when the light and heavy fragments respectively are moving towards the detector D_2. It can be seen from Fig. 1 that when the fragments are moving towards the detector D_2, the x-rays emitted all along the fragment path are not seen by the x-ray detector. Therefore only the first hump in $Y_x^L(M)$ and the second hump in $Y_x^H(M)$ correspond to the unshielded view, while the other two humps correspond to a partially shielded view. The data have been analysed to obtain the observed K x-ray yield per fragment for the cases of unshielded and partially shielded views separately.

The unbiased and mass distribution $Y(M)$ and the distribution $Y_x(M_{L,H})$ in coincidence with the light or heavy fragment K x-rays are related by

$$Y_X(M_{L,H})/Y(M) = \Omega\,\eta(M_{L,H})\,N_X(M_{L,H}) = R_X(M_{L,H}) \qquad \ldots.(1)$$

where $N_X(M_{L,H})$ is the average number of K x-rays emitted from masses $M_{L,H}$, $\eta(M)$ is the detection efficiency for the K x-rays characteristic of fragment mass M, and Ω is the solid angle of detection. Thus, $R_X(M_L)$ and $R_X(M_H)$ were obtained from channel by channel division of the counts in the 2/4 and 3/4 respectively by the counts in the 1/4 of the analyser memory. The values of $R_X(M)/\Omega$ are plotted as a function of final fragment mass M_f (after neutron emission and corrected for mass dispersion) in Fig.5(a). The solid angle of detection Ω was calculated for the present experimental geometry with the computer CDC-3600 using a Monte Carlo method, taking into account the finite size of the source and x-ray detector. Since the direction of fragment motion is perpendicular to the direction of x-ray detector and the x-ray detector was at a relatively large distance as compared to the foil-fragment detector distance (Fig.1), the solid angle was calculated assuming that all the x-rays were emitted at the source foil itself. This approximation can only lead to a maximum uncertainty in the calculated solid angle of about 3% which is included in the quoted results.

Corrections for the Energy Resolution of X Ray Detector

The determination of $N_X(M_{L,H})$ from Eq.(1) is valid only if the pulse height selected from the single channel window settings always correspond to the energy windows of 8 - 21 kev and 21 - 50 kev required for separating K x-rays from the light and heavy fragment groups. However, due to a pulse height spread in the x-ray detector output, the pulse height distribution of the heavy fragment x-rays has a tail extending into the light fragment x-ray window and vice versa. In addition, the escape peak of the heavy fragment x-rays of energies greater than 32 kev falls in the light fragment x-ray region. The values of $N_X(M_{L,H})$ corrected for these effects were derived in the following manner:

Let $P^R(M)$, $P^W(M)$ and $P^o(M)$ be the probabilities that x-ray emitted from mass M gets detected and gives a pulse height falling in the right window, wrong window, and outside the window ranges respectively. Then,

$$P^R(M) + P^W(M) + P^o(M) = \eta(M)\cdot\Omega \qquad ......(2)$$

The values of $N_X(M_L)$ and $N_X(M_H)$ for a pair of complementary fragments are then related to the measured values $R_X(M_L)$ and $R_X(M_H)$ by the following equations:

$$R_X(M_L) = N_X(M_L)\ P^R(M_L) + N_X(M_H)\ P^W(M_H) \qquad ......(3)$$

and

$$R_X(M_H) = N_X(M_H)\ P^R(M_H) + N_X(M_L)\ P^W(M_L) \qquad ......(4)$$

The probabilities $P^R(M)$ and $P^W(M)$ were calculated using the measured response of the NaI detector for different photon energies. It was found that the experimental energy resolution (full width at half maximum, FHWM) as a function of energy E_X has the simple relation, FWHM = $a\ E_X + C$, where a and c are constants.

With this relation, Gaussian distributions of average K x-ray energies equal to those expected for emission from different fragment masses, and having areas equal to $\eta(M).\Omega$ were computed. To calculate average K x-ray energy from fragment mass M, the corresponding fragment charge was calculated on the equal charge displacement hypothesis[11]. The efficiency of the 1 mm NaI crystal for different energies was calculated from the known photo-electric and total absorption cross sections also taking into account a small attenuation of the x-rays in the two beryllium windows. For x-ray energies greater than 32 kev, the resulting pulse height distributions were taken as two separate Gaussians of average energies E and (E-28) kev, and having areas equal to $\eta(M)\Omega\{1-p(M)\}$ and $\eta(M)\Omega\, p(M)$ respectively where p(M) is the escape probability for x-rays emitted from mass M. The areas under the two Gaussians in the ranges 8 - 21.0 kev and 21.0 - 50 kev where computed by numerical integration to obtain the values of $P^R(M_L)$, $P^W(M_L)$, $P^R(M_H)$ and $P^W(M_H)$. The number $N_X(M)$ of K x-rays per fragment obtained from Eqs.(3) and (4) are plotted against the fragment mass M_f after neutron emission in Fig. 5(b), both for the cases of unshielded and partially shieded views. The K x-ray yields per fragment for different fragment masses shown in Fig.5 have been corrected for the effects of experimental mass resolution in an average manner by plotting the yield at the mass corrected for the mass dispersion shift. Consequently, the x-ray yield for any mass M_f should be interpreted to represent a weighted average yield over a few neighbouring fragment masses. The observed smooth variation of the yield with fragment mass therefore does not rule out the possibility of different K x-ray yield from neighbouring odd and even masses. Nevertheless, the present results do show the average behaviour of the variation of the K x-ray yield as a function of fragment mass for U^{236} fragments similar to the earlier measurements[1,2] for Cf^{252} fragments.

From the measured yield per fragment for the unshielded view, the average number of K x-rays emitted from the light and heavy groups were calculated and the values are given in Table-I. The results of other measurements are also shown in the table for comparison. From the present data the average number of K vacancies per fission is calculated to be (0.12 + 0.01) for the light group and (0.35 + 0.02) for the heavy group. The ratio of the observed number of K x-rays for the unshielded and shielded views are found to be (1.42 $\pm$ 0.09) and (1.54 $\pm$ 0.09) for emission from the light and heavy groups respectively. From the experimental geometry it is found that in the case of partially shielded view, the observed yield refers to only those x-rays emitted in the initial 0.9 cm of the fragment path. On this basis, the observed ratios correspond to average x-ray half lives of (0.36 $\pm$ .05) nsec. and (0.62 $\pm$ .07) nsec. for the light and heavy groups respectively, assuming a single decay constant. It may, however, be noted that the assumption of a single decay constant is an unrealistic one. In fact a continuous spectrum of various half-life components can be expected for each fragment group firstly due to different possible gamma half-lives and secondly due to different values of conversion coefficients. The half-lives estimated here, therefore, correspond to a suitably weighted average over the fragment group of the product of gamma half life and the corresponding internal conversion probability for different transitions.

IV DISCUSSION

For the purpose of comparison, the present results on K x-ray yield from U^{236} fragments (unshielded view) are shown in Fig. 5 together with the previously[2] measured K x-ray yield from Cf^{252} fragments. Since the light peak of the mass distribution is at a lower mass in the fission of U^{236} as compared to that in the fission of Cf^{252}, in this work it has been also possible to obtain data for fragment masses less than 90 in the region of neutron closed shell of N=50 for which no data were available from Cf^{252} studies. The K x-ray yield curve for Cf^{252} has been earlier[1-4] interpreted on the basis of the variation of the internal conversion probability as a function of mass as expected from the characteristics of the low lying states. The present results on the yield from U^{236} fragments are consistent with the interpretations earlier put forward for the case of Cf^{252}. As expected, the x-ray yield is found to be vanishingly small for fragments of mass around 84 which have closed neutron shell of N = 50. As one moves away from this closed shell, the yield is found to increase upto mass 106, similar to the case of emission from Cf^{252} fragments. Since both the U^{236} and Cf^{252} fragments are neutron rich to nearly the same extent, the present results are consistent with the proposal[12, 2-4] that the neutron rich fragments around mass 106 make up a new region of deformation and therefore deexcite with lower energy, highly converted transitions. However, an alternative explanation for the observed high K x-ray yield in this region could be that in the neutron rich even nuclei around mass 106 the first excited state is 0^+ leading to $0^+ \longrightarrow 0^+$ transitions.

For the heavy group of U^{236} fragments, the minimum in the yield is also found to be in the region of closed Z = 50 and N = 82 shells, similar to the case of Cf^{252}. However, the striking increase in the yield for masses greater than 144 (corresponding to $N > 88$) observed for the case of Cf^{252} does not seem to be apparent for the case of U^{236}. On the other hand the yield from U^{236} fragments appears to be nearly constant or somewhat decreasing with increasing mass for fragment masses between 144 and 151. This effect appears to be similar to that earlier reported[1,2] for Cf^{252}, where a drop in the yield beyond mass 153 was observed, although the region of stable deformation is known to extend to mass 180. Atneoson et al[3] have pointed out that this drop in the yield may be connected with the possibility that these fragments ($M_f > 153$) are not being formed with sufficient spin to undergo a cascade of rotational transitions. It has been suggested that closed shell spherical nuclei which cannot receive spin by simple Coulomb interaction may also be less effective in imparting spin to the partner fragment which may be deformed. Consequently, fragments of masses greater than 153 may be formed with continually decreasing spin as these fragments at scission will be paired off with fragments approaching spherical shape, due to the proximity with N = 50 shell. It is possible to test these arguments by a comparison of the K x-ray yield for U^{236} and Cf^{252} fragments, since mass of the heavy fragment paired off with the light fragment having N = 50 is different in the two cases. On the basis of the observed[13] number of neutrons as a function of fragment mass we assume that due to neutron closed shell at N = 50, the scission deformation of the light fragment is continuously decreasing below mass 97 and 90 for the cases of Cf^{252} and U^{236} fragments respectively. The corresponding masses of the partner heavy fragments after neutron emission are 152 and 144 respectively in the two cases. It can therefore be expected that the spin imparted to the heavy fragment decreases as one moves beyond these masses. The drop in the x-ray yield for Cf^{252} fragments does indeed appear at about mass 153. For emission from U^{236} fragments also, the points in Fig. 4(b) can be interpreted either to suggest a decrease in the yield beyond mass 144 or at least a constant yield between masses 144 to 151. It therefore appears quite likely that the absence of a striking increase in the x-ray yield for masses beyond 144 (corresponding to $N \sim 88$) for the case of U^{236} fragments is due to the pairing off of these fragments with undeformed partners having $N \sim 50$. The present results, therefore, favour the argument that the x-ray yield depends both on the properties of the low lying states and the initial spin of the fragment. It may be pointed out that in some recent determinations[4] of the K x-ray yield from Cf^{252} fragments as a function of fragment atomic numbers, the decrease in the K x-ray yield for $Z > 60$ corresponding to $M_f > 153$ is not evident. If this observation does not arise due to any uncertainties in the fragment charge yield curve used for the above determination, one has to assume that the shapes of the K x-ray yield curve differ when plotted as a function of fragment mass and atomic number. It will be interesting to determine with a high resolution Li-drifted silicon detector the K x-ray yield as a function of fragment charge for U^{236} fragments to see whether such a difference is apparent in this case also. The above arguments based on the role of initial spin of the fragments are valid only if the variation of the K x-ray yield as a function of fragment atomic number is similar to that as a function of mass number.

V. ACKNOWLEDGEMENTS

We are extremely thankful to Dr. R. Ramanna for his keen interest in the work and for several helpful discussions. Help from S.R.S. Murthy and P.N. Rama Rao in the carrying out of the experiments and in the maintenance of the electronic equipments is gratefully acknowledged. Thanks are due to S.K. Kataria for his help with the computer calculations and for other useful suggestions. One of us (R. Zaghloul*) wishes to thank Bhabha Atomic Research Centre, Trombay, U.A.R. Atomic Energy Establishment, Cairo and the International Atomic Energy Agency for getting the opportunity to work at this laboratory.

---

* On leave from U.A.R. Atomic Energy Establishment, Cairo, Present address: Reactor Physics Group, A.E.E., Cairo, U.A.R.

APPENDIX I

Mass Calibration and Correction for Mass Dispersion

The fragment masses are derived from the fragment kinetic energies with the momentum conservation relation. If E_1^* and E_2^* are the fragment kinetic energies before neutron emission, it follows that

$$M_1 = 236 \frac{E_2^*}{E_1^* + E_2^*}$$

The effect of neutron emission on the mass distribution arises from the following two factors; Firstly, it introduces a dispersion in the fragment mass because of the variation in the neutron number, direction and energy. This dispersion increases[13] the variance of the mass distribution by about (2.8) (mass unit)^2. Secondly, the calculated mass M_1^c obtained from the ratio $E_1/(E_1 + E_2)$ will be shifted with respect to the actual mass depending on the number of neutrons emitted. The difference between the calculated mass M_1^c and actual mass M_1 is given by

$$M_1^c - M_1 = (M_2 \nu_1 - M_1 \nu_2)/236 \qquad \ldots\ldots(1)$$

where ν_1 and ν_2 are the number of neutron emitted by fragments 1 and 2.

On the basis of available data, the pulse height from the fragment detector varies linearly[14] with fragment energy and mass. In this case, the pulse height ratio $V_2/(V_1 + V_2)$ also varies linearly[3] with the energy ratio $E_2/(E_1 + E_2)$ and consequently distribution in the pulse height ratio gives the distribution of the fragment mass M_1^c.

For the mass calibration, the calculated masses M_1^c for the two peaks and one minimum of the mass distribution curve were ascertained from the data of Schmitt et al[15]. The channel numbers corresponding to the same points in our mass yield data were ascertained and a least square fit gave the relationship between calculated masses and channel number.

The mass distributions thus obtained are shown in Fig.4, where the fragment mass refers to that uncorrected for the effects of neutron emission and mass dispersion. The variance of the observed binary mass distribution is about 65 (mass unit)^2 indicating a variance of about (15.8) (mass unit)^2 for the mass dispersion function which is attributable largely to the instrumental effects. Correction for the experimental mass dispersion shift was carried out using the method of Terrell[13]. The initial fragment masses corresponding to the new calculated masses corrected for the mass dispersion shift were obtained with Eq.(1). The experimental mass yield curve corrected for mass dispersion effects is compared with that obtained by Schmitt et al[15] in Fig.7. The observed good agreement between the two curves ensures the consistency of the procedure adopted for mass calibration and dispersion correction. The final fragment masses M_f representing the masses of fragment nuclei undergoing gamma deexcitation were obtained by substracting the number of neutrons emitted from different masses.

TABLE I

The Light- and Heavy-fragment K x-ray Yield for U^{236} Fission Fragments

Light-fragment yield (K x-rays/fission)	Heavy-fragment yield (K x-rays/fission)	References
(0.08 ± 0.01)	(0.30 ± 0.02)	Present work
(0.10 ± 0.03)	(0.42 ± 0.12)	5
0.08	0.12	6
(0.17 ± 0.02)	(0.43 ± 0.04)	7
(0.12 ± 0.03)	(0.20 ± 0.05)	8
(0.18 ± 0.06)	(0.39 ± 0.09)	9

REFERENCES

1. L.E. Glendenin and H.C. Griffin; Phys. Letters 15, 153 (1965).
L.E. Glendenin and J.P. Unik; Phys.Rev. 140, B 1301 (1965).
2. S.S. Kapoor, H.R. Bowman and S.G. Thompson; Phys.Rev. 140, B 1310 (1965).
3. R.A. Atneoson, T.D. Thomas, W.H. Gibson and M.L. Perlman; Phys.Rev. 148, 1206 (1966).
4. R.L. Watson, H.R. Bowman and S.G. Thompson; Phys.Rev. 162, 1169 (1967).
5. V.V. Sklyarevskii, E.P. Stepanov, and B.A.Medvedev; JETP 9, 225 (1959).
6. H. Hohman; Z.Physik 172, 143 (1963).
7. L. Bridwell, M.E. Wyman and B.W. Wehring; Phys.Rev. 145, 963 (1966).
8. B.W. Wehring and M.E. Wyman; Phys.Rev. 157, 1803 (1967).
9. V.P. Eismont and Yurgenson; Soviet Journal of Nucl. Phys. 5, 852 (1967).
10. R. Zaghloul; "Ph.D. Thesis", University of Bombay, India, 1968.
11. L.E. Glendenin, C.D. Coryell, and R.R. Edwards; in Radiochemical Studies: the fission Products, edited by C-C. Coryell and N. Sugarman (McGraw-Hill Book Company, Inc., New York, 1951), p. 489.
12. S.A.E. Johansson; Nuclear Physics 60, 378 (1964).
13. J. Terrell, Phys.Rev. 127, 880 (1962).
14. H.W. Schmitt, W.H. Gibson, J.H. Neiler, F.J.Walter and T.D.Thomas; "Physics and Chemistry of Fission", Vol.1, 531, IAEA, Vienna, 1965.
15. H.W. Schmitt, J.H. Neiler and F.J. Walter; Phys.Rev.141, 1148 (1966).

FIGURE CAPTIONS

Fig. 1 Schematic diagram of the experimental arrangement for determining the K x-ray yield from different fragments.

Fig. 2 Block diagram of the electronic arrangement for K x-ray yield determination.

Fig. 3 The energy distribution of the K x-rays after correction for background. In this measurement, the x-ray detector was placed on the other side of the foil in line with the fragment detector.

Fig. 4 The mass distributions observed in coincidence with the light and heavy group of K x-rays are shown along with the observed unbiased mass distribution. The shaded humps correspond to the partially shielded view of the x-ray detector, while the other two humps are for the unshielded view.

Fig. 5(a) Measured K x-ray yield uncorrected for detection efficiency and the effects of energy resolution of the x-ray detector is plotted as a function of fragment mass after neutron emission (corrected for mass dispersion shift).

Fig. 5(b) Number of K x-rays per fragment after correction for detection efficiency and the energy resolution effects is plotted as a function of fragment mass after neutron emission (corrected for mass dispersion shift).

Fig. 6 A comparison of K x-ray yield from U^{236} and Cf^{252} fragments.

Fig. 7 Mass distribution curve obtained with the adder-divider circuit and after corrections described in the Appendix is compared with the measurements of Schmitt et al[15].

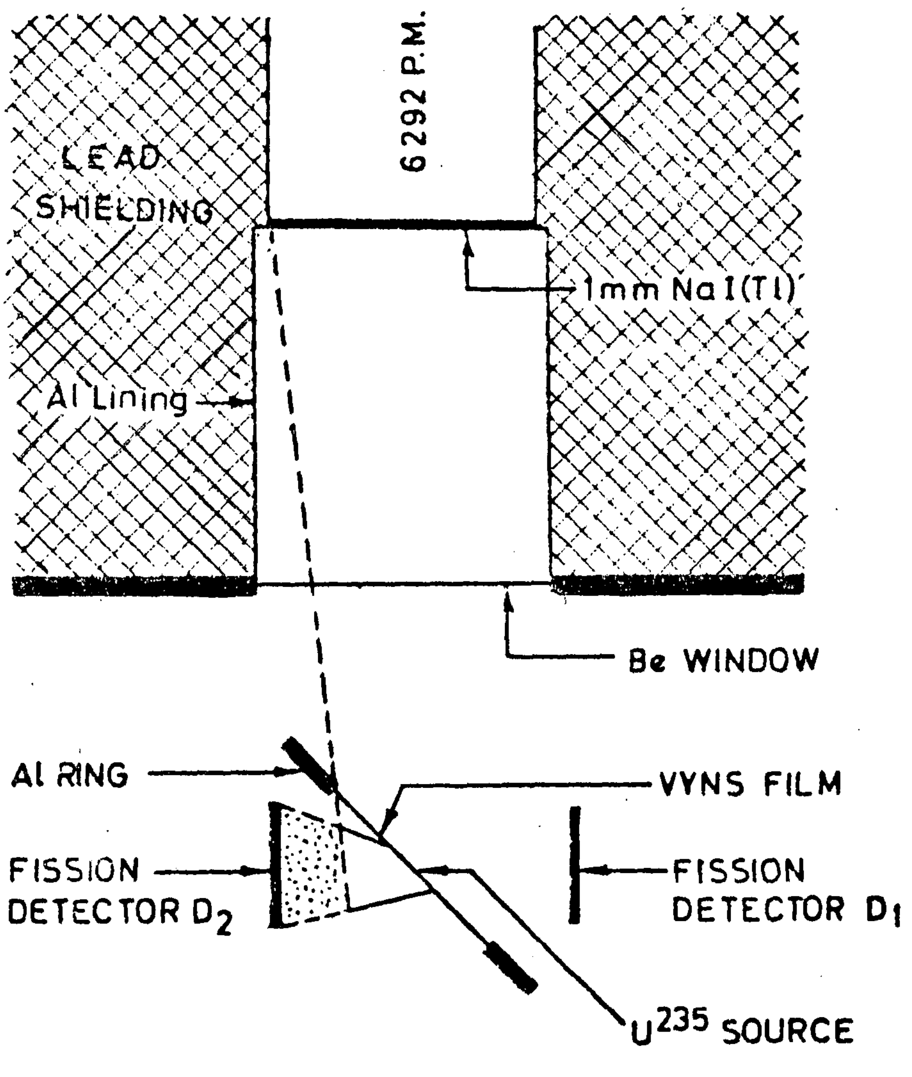
6292 P.M.
LEAD
SHIELDING
1mm NaI(Tl)
Al Lining
Be WINDOW
Al RING
VYNS FILM
FISSION
DETECTOR D2
FISSION
DETECTOR D1
U235 SOURCE

Fig 1.

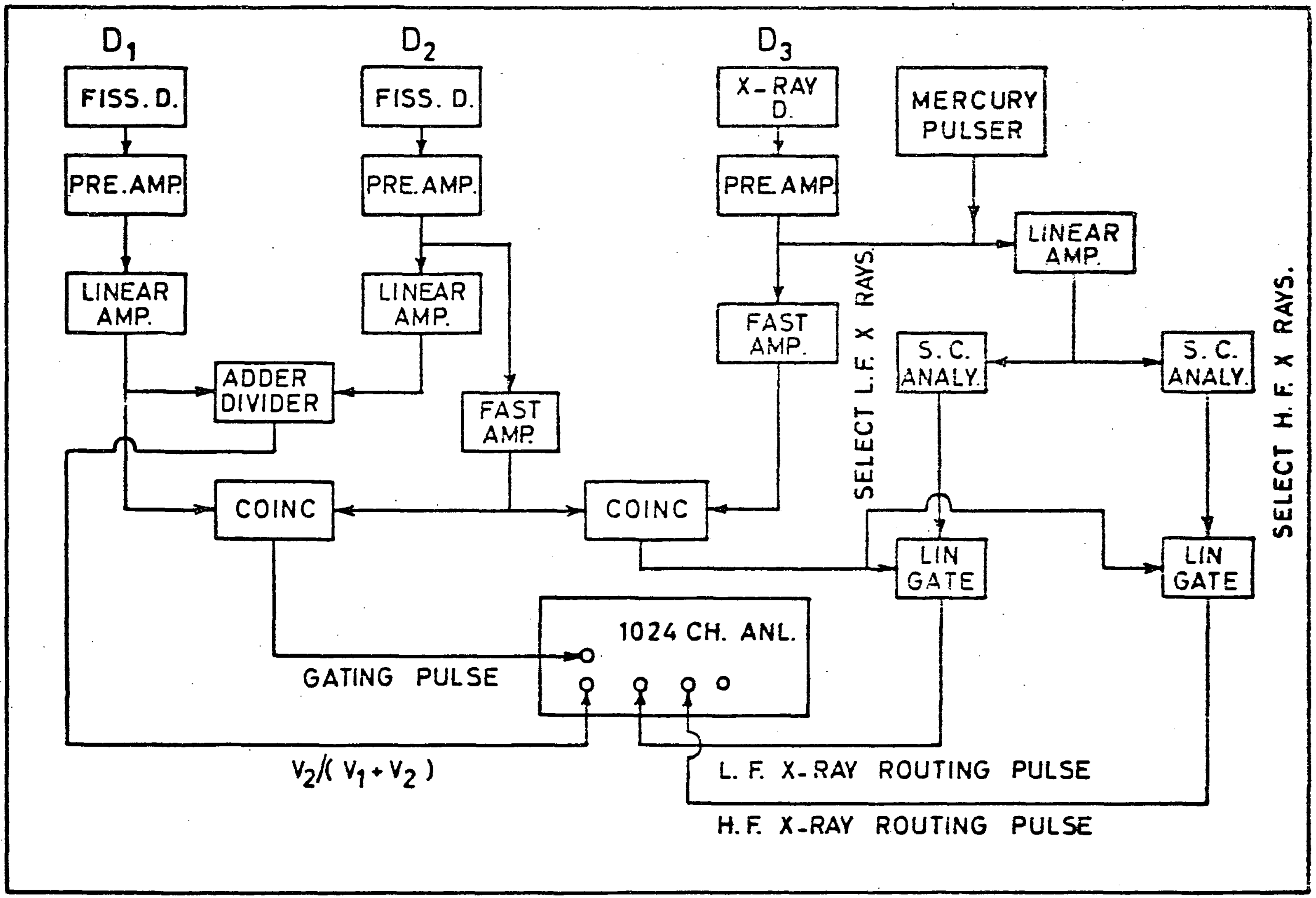
D1
D2
D3
FISS. D.
FISS. D.
X-RAY D.
MERCURY PULSER
PRE. AMP.
PRE. AMP.
PRE. AMP.
LINEAR AMP.
LINEAR AMP.
LINEAR AMP.
ADDER DIVIDER
FAST AMP.
FAST AMP.
S. C. ANALY.
S. C. ANALY.
SELECT L.F. X RAYS.
SELECT H. F. X RAYS.
COINC
COINC
LIN GATE
LIN GATE
1024 CH. ANL.
GATING PULSE
V2/(V1 + V2)
L. F. X-RAY ROUTING PULSE
H. F. X-RAY ROUTING PULSE

Fig 2.

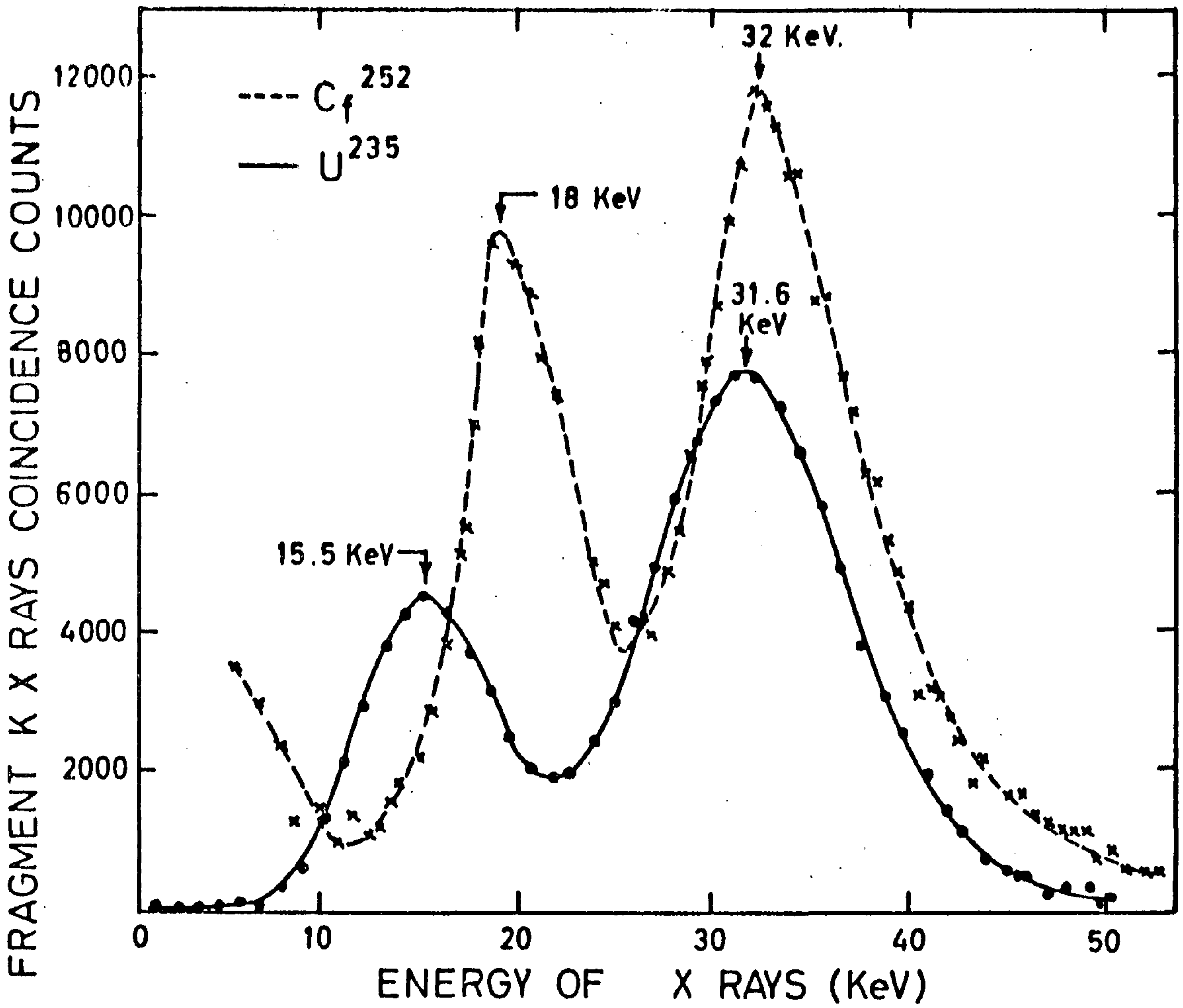
FRAGMENT K X RAYS COINCIDENCE COUNTS
ENERGY OF X RAYS (KeV)
Cf 252
U 235
32 KeV.
18 KeV
31.6 KeV
15.5 KeV
12000
10000
8000
6000
4000
2000
0
10
20
30
40
50

Fig 3.

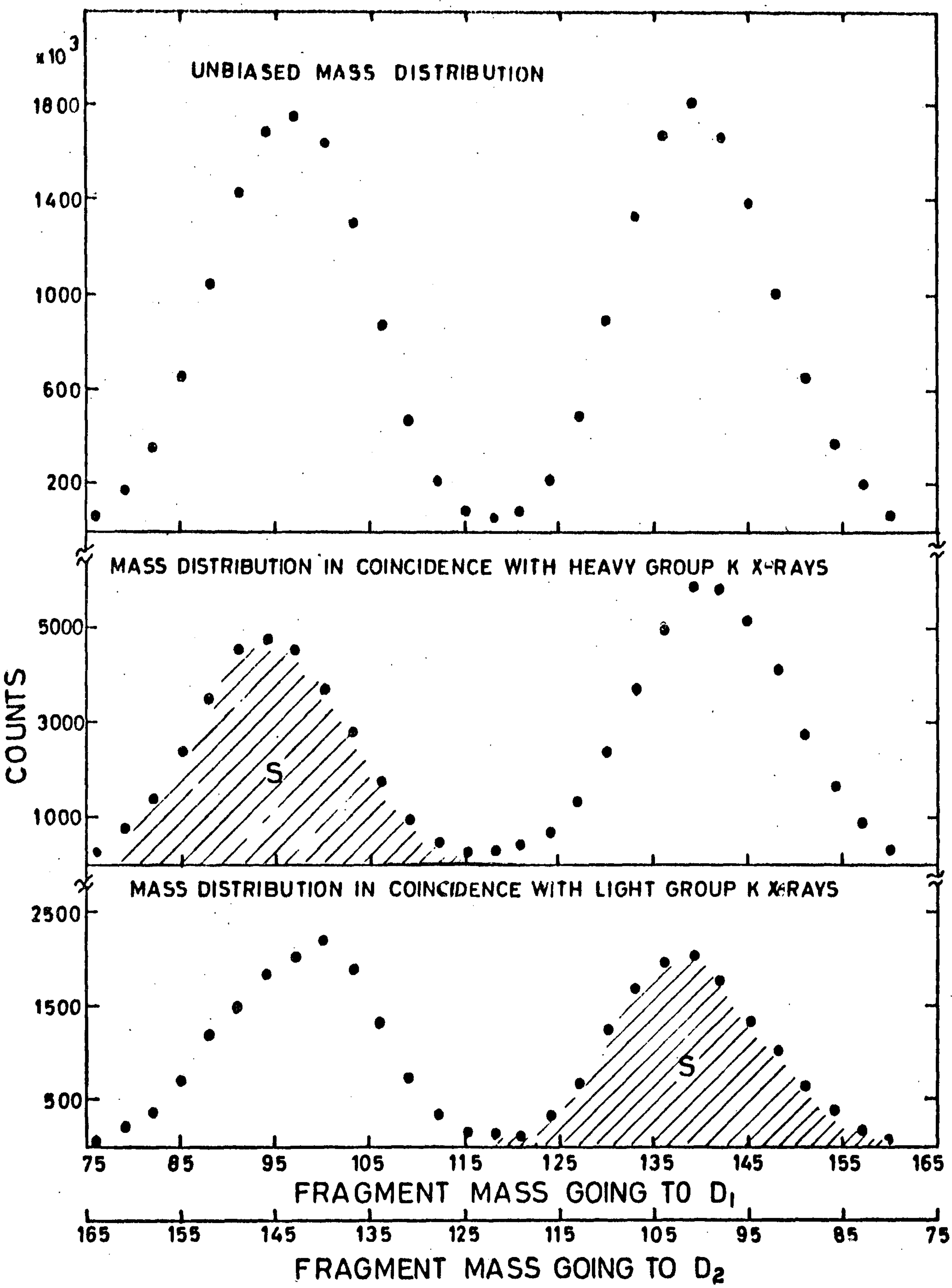

x10³
UNBIASED MASS DISTRIBUTION
1800
1400
1000
600
200
MASS DISTRIBUTION IN COINCIDENCE WITH HEAVY GROUP K X-RAYS
5000
3000
1000
S
COUNTS
MASS DISTRIBUTION IN COINCIDENCE WITH LIGHT GROUP K X-RAYS
2500
1500
500
S
75 85 95 105 115 125 135 145 155 165
FRAGMENT MASS GOING TO D1
165 155 145 135 125 115 105 95 85 75
FRAGMENT MASS GOING TO D2

Fig 4.

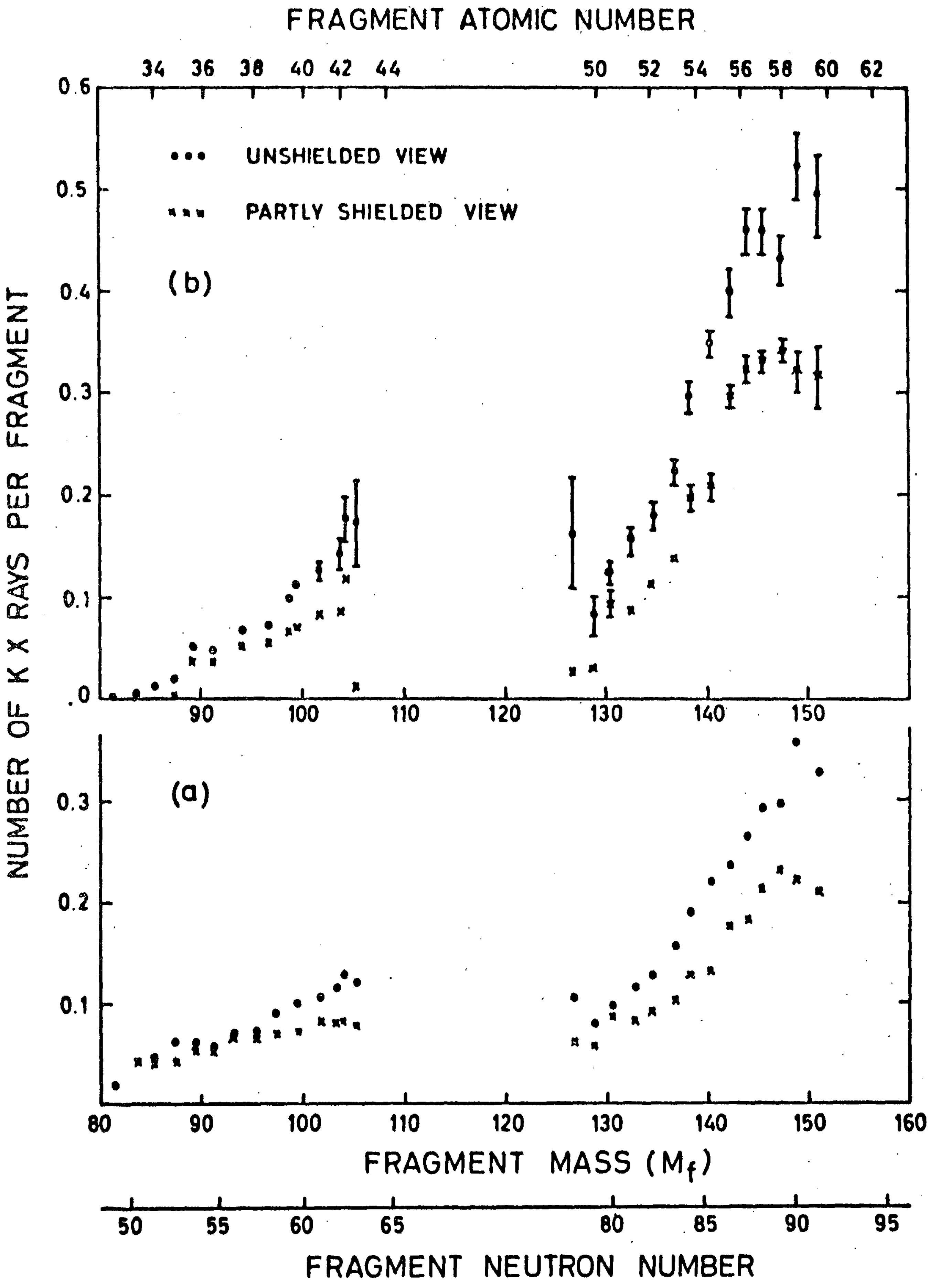
FRAGMENT ATOMIC NUMBER
34 36 38 40 42 44 50 52 54 56 58 60 62
UNSHIELDED VIEW
PARTLY SHIELDED VIEW
(b)
(a)
NUMBER OF K X RAYS PER FRAGMENT
0.6
0.5
0.4
0.3
0.2
0.1
.0
90 100 110 120 130 140 150
80 90 100 110 120 130 140 150 160
FRAGMENT MASS (M_f)
50 55 60 65 80 85 90 95
FRAGMENT NEUTRON NUMBER

Fig 5.

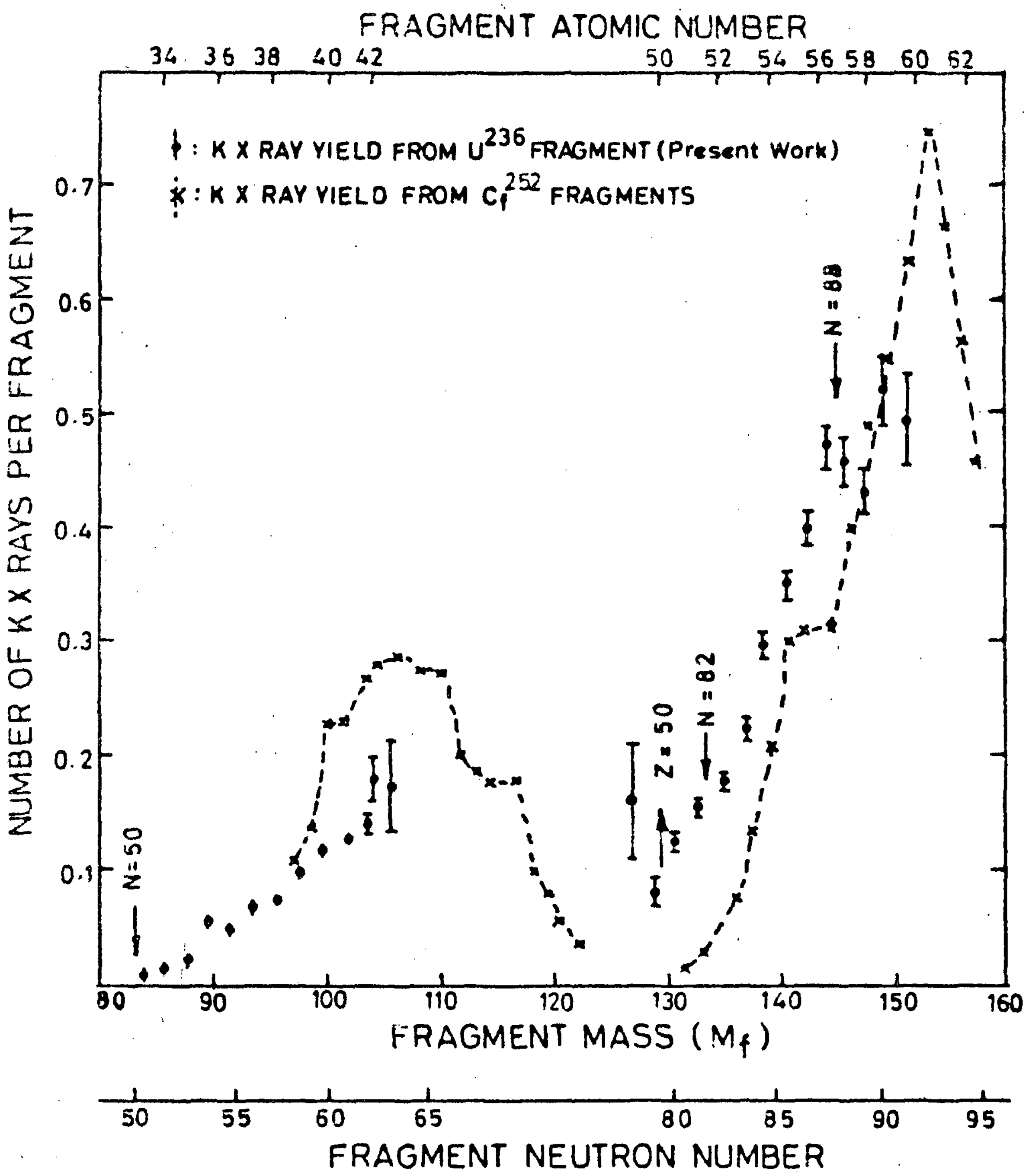
FRAGMENT ATOMIC NUMBER
34 36 38 40 42 50 52 54 56 58 60 62
: K X RAY YIELD FROM U^{236} FRAGMENT (Present Work)
: K X RAY YIELD FROM C_f^{252} FRAGMENTS
NUMBER OF K X RAYS PER FRAGMENT
0.7
0.6
0.5
0.4
0.3
0.2
0.1
N=50
Z=50
N=82
N=88
80 90 100 110 120 130 140 150 160
FRAGMENT MASS (M_f)
50 55 60 65 80 85 90 95
FRAGMENT NEUTRON NUMBER

Fig 6.

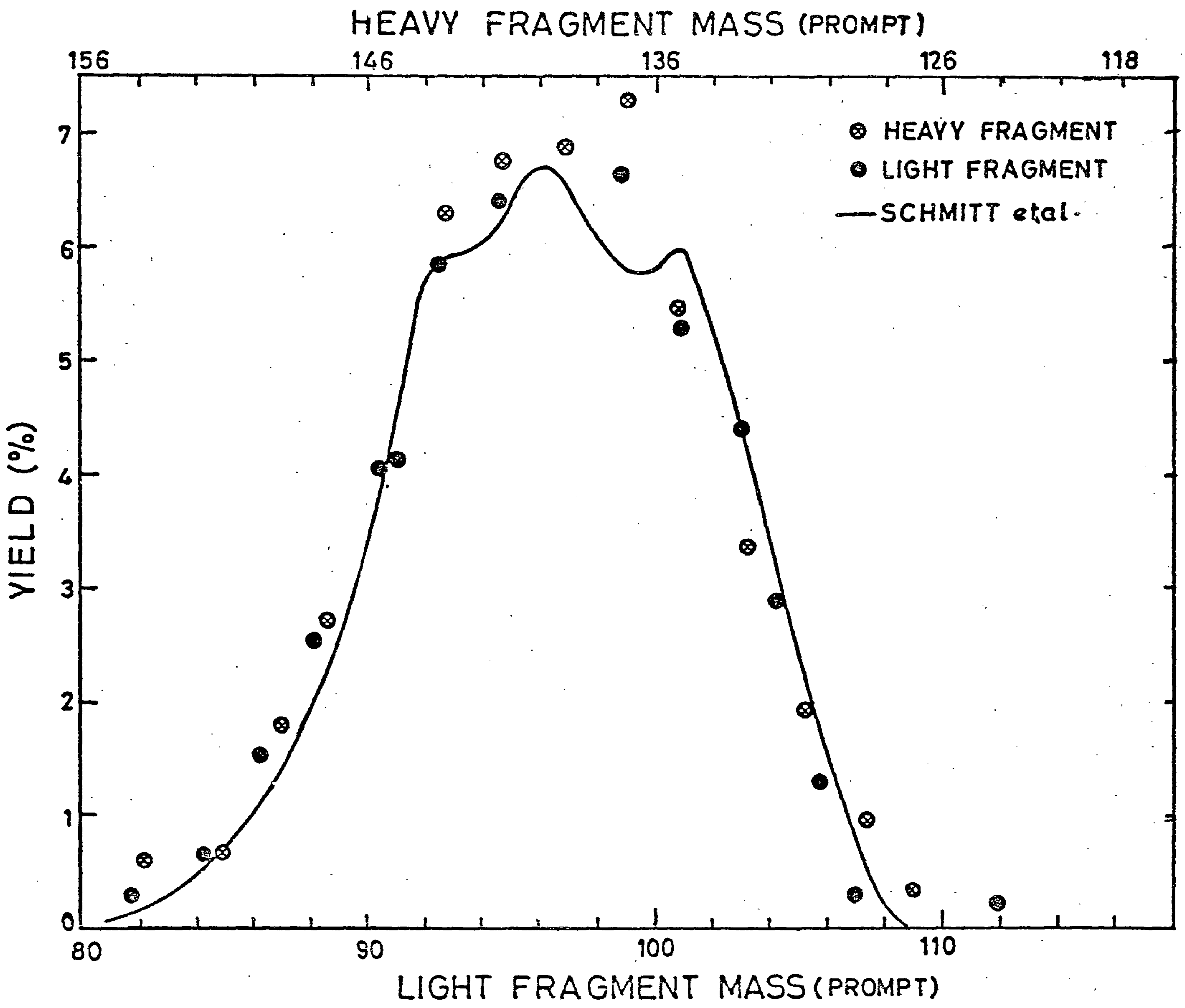
HEAVY FRAGMENT MASS (PROMPT)
156
146
136
126
118
HEAVY FRAGMENT
LIGHT FRAGMENT
SCHMITT etal.
YIELD (%)
0
1
2
3
4
5
6
7
80
90
100
110
LIGHT FRAGMENT MASS (PROMPT)

Fig 7.